Novel *H*-type rf deflector

Yu. Senichev,[1] O. Belyaev,[2] W. Bräutigam,[1] Yu. Budanov,[2] R. Maier,[1] V. Stepanov,[2] V. Teplyakov,[2] A. Zherebtsov,[2] and I. Zvonarev[2]

[1]*FZJ, Institute of Nuclear Physics, D-52425, Juelich, Germany*
[2]*Institute of High Energy Physics, Protvino, Russia*

(Received 6 October 2005; published 31 January 2006)

In this work we developed a new rf deflector based on the *H* resonator, which differs from previous ones in its design, the type of rf fundamental mode and the possibility of providing the π-mode standing wave for the beam in the deflection system. Because of the last aspect, the transverse shunt impedance of this deflector is much higher in comparison with its analogues. This idea was originally intended for application in the funneling system of the European Spallation Source, but we later found many additional applications, in particular, as the bunch separator after the electron and proton linear accelerators. We studied the beam dynamics and the electrodynamics and optimized the device parameters in the assumed range of frequency of 150–700 MHz for the proton beam and 1000–1500 MHz for the electron beam. To make the final choice we analyzed rf deflectors of different designs. We manufactured the experimental sample tested at the low rf power level.

DOI: 10.1103/PhysRevSTAB.9.012001 PACS numbers: 29.17.+w, 29.27.Ac, 41.85.Ja, 41.90.+e

I. INTRODUCTION

In previous papers [1–3] the idea of the resonant multielectrode funneling system based on an *H*-type structure has been developed. The distinctive feature of this system is the very simple cavity design, providing the π-mode standing wave for the beam with high transverse shunt impedance, and this principle can be realized in the wide rf range of 150–1500 MHz. It was intended for application in the European Spallation Source [4]. Since the individual *H* source cannot provide the required intensity of $\sim$100 mA, two identically bunched beams have to be merged into a single beam with double intensity.

The idea of merging the beam was first proposed by Montague and then by Bongardt with Sanitz [5], and called the funneling system. Walling provided the first design for the rf facility [6] based on the coaxial $\lambda/2$ cavity, and the funneling was tested for the first time in Los Alamos by Stovall [7]. Krawczyk and Kurennoy improved the coaxial cavity [8] to increase the shunt impedance. Schempp proposed using two radio frequency quadrupoles (RFQs) as the transport channels to the deliver the beams to the rf deflector with the $\beta\lambda$ profiled electrode [9], and later it was suggested that the drift tube should be used to increase the bunch deflection efficiency [10]. In all of these versions the funneling system has one pair of electrodes, providing in the best case the 0-mode standing wave for the beam [9,10]. Therefore they all have low transverse shunt impedance and are restricted to having a large deflection angle.

We propose the resonant method of beam funneling based on the multielectrode system providing for the π-mode standing wave. We analyzed, designed and compared at least four different types of *H* cavities giving the effective resonant merging of beams. Additionally, instead of the pulse method for dividing the beam into two rings (or more for multipurposes facilities) we suggest using our device to split the beam after acceleration into two or three beams and to deliver them to the different facilities simultaneously, for instance, upon injection into the SNS ring, or for use in the switchyard in the TESLA facility.

Since the frequencies of chain bunches and the rf deflector resonator have to be divisible by factor ≥ 2, we considered two frequency ranges: 150–700 MHz for the proton accelerator and 1000–1500 MHz for the electron accelerator.

II. DIFFERENT TYPES OF RF DEFLECTORS

In general, there are two possible solutions for deflecting the beam: HEM mode excitation in the traveling wave structure, such as the Panofsky-type rf beam separator [11], and the standing wave structure with the transverse electrical component, for instance, the coaxial $\lambda/2$ cavity [6–8] and its modification. The first solution is widely used in the short-pulse electron accelerator, but it is not applicable for high duty cycle machines, since it requires a high-power generator. Therefore resonant systems are preferable in the proton machines. Figure 1 shows schematics of three types of rf deflector: the half-wave coaxial [6–8], the profiled electrode coaxial [9,10], the multielectrode system [1–3].

The Los Alamos single-gap deflector is essentially a capacitively loaded, $\lambda/2$ odd-mode resonator [see Fig. 1(a)]. The electric field in the gap transverse to the beam direction was designed to merge two incoming beams with an energy of 20 MeV by bending each of them 1.3° in the required direction. In order to achieve the desired efficiency of the beam interaction with the electric field the drift tubes were installed from both ends

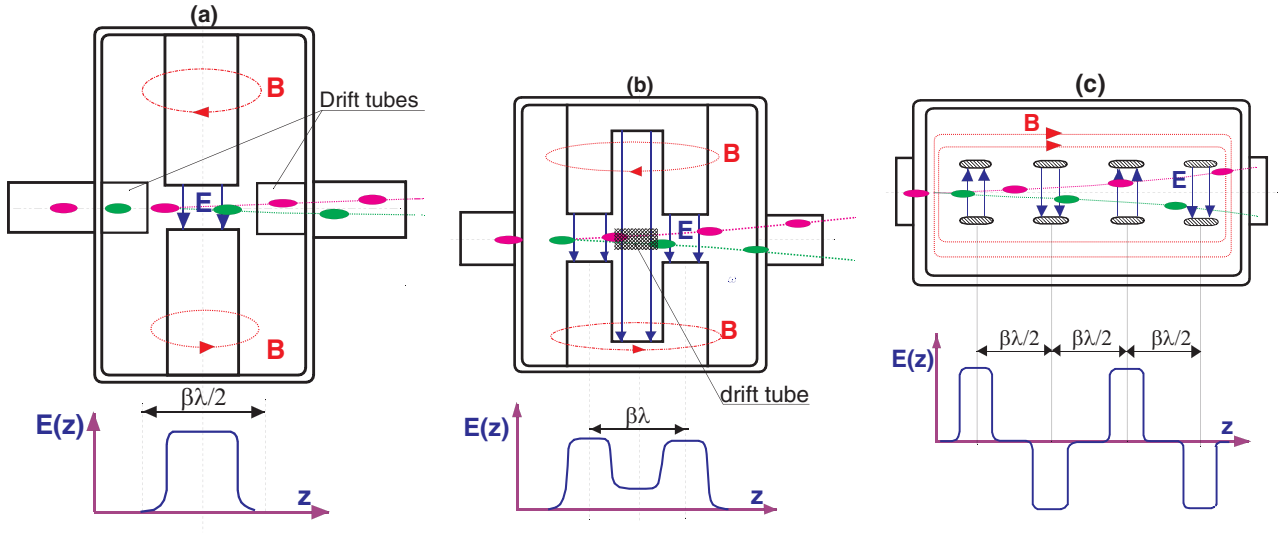

FIG. 1. (Color) Three types of rf deflectors: the half-wave coaxial (a), the profiled electrode coaxial (b), the multielectrode system (b).

of the gap. As a result, the deflector has one gap $\beta\lambda/2 =$ 7.6 cm in length along the whole path of 23 cm crossing through the cavity [8].

The required peak transverse electric field in the center of the gap is about 20 MV/m. In such an rf device the large metallic surface surrounds one electric gap, and therefore the high rf field dramatically increases the rf losses up to 50 kW in the CW regime.

The profiled electrode shown in Fig. 1(b) without the drift tube has low efficiency due to the negative effect of the farthest part of the electrode. In the case of the additional drift tube together with the supporting bar the total shunt impedance is evidently reduced.

We developed the rf deflector based on the new principle. Figure 1(c) shows schematically the main idea of the multielectrode system. It is based on either TE211 mode [Fig. 2(a)], or TE111 mode [Fig. 2(b)], or TE101 mode for the rectangular cavity [Fig. 2(c)]. The pair of electrodes has the shape of the usual capacitor with the plates shifted relative each to other in a direction perpendicular to the beam. Their position is alternately changed along the cavity [see Figs. 2(a)–2(c)]. The magnetic field has either two variations [see Fig. 2(a)] or one [see Figs. 2(b) and 2(c)] variation in the transverse direction and surrounds all the electrodes in the longitudinal direction from above to below. The electric field has to be perpendicular to the magnetic field and it is directed along the electrodes. At the location where one electrode comes over another, the induced electric field arises in the gap between them, and it is directed bottom-up. For the next pair, the position of the electrodes is changed, and the induced electric component flips to the bottom.

In comparison with the two previous coaxial options, the H-type rf deflector creates the π transverse mode and deflects the beam on each $\beta\lambda/2$. Because of this fact alone the shunt impedance is already twice as great.

III. ELECTRODYNAMICS OF *H*-TYPE RF DEFLECTOR

At the beginning of our investigation, we considered different resonators of a cylindrical and rectangular shape

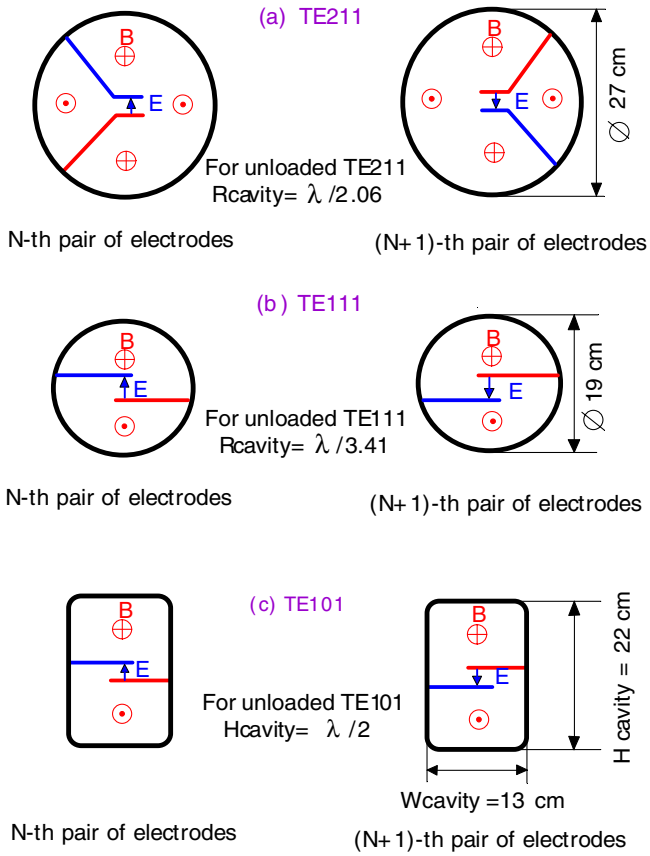

FIG. 2. (Color) (a)–(c) Possible rf deflector structure.

with the different fundamental modes TE211 and TE111, or TE101 [1,2]. In the empty cylindrical cavity without any electrodes inside (unloaded cavity) the critical wavelength of the TE211 and TE111 modes is related to the radius of the cavity by the ratio $R = \lambda/2.06$ and $R = \lambda/3.41$, respectively. In the rectangular shape, the critical wavelength of the TE101 mode is twice as great as the cavity height. To provide the transverse electric field we installed the electrodes inside the cavity, and these electrodes obviously carry in the capacity. As a result, the total frequency decreases. To compensate the frequency decrease the radius of the cavity has to be reduced as well.

Figures 2(a)–2(c) show cross sections at the location of two neighboring pairs in the possible resonators with electrodes for the frequency 352 MHz. It can be seen that for the lower frequency range of 150–700 MHz the TE111 (or the TE101) are preferable and the TE211 can be used at the higher frequency >1500 MHz.

The insertion of electrodes into the cavity breaks the axial symmetry and later motivated us to move on to the rectangular option. Figure 2(c) shows the cavity based on the TE101 mode. The height of the cavity for this mode is roughly the average of the TE211 and TE111 modes. Besides, due to the magnetic field distribution, the rectangular cavity has a more convenient design for the tuning and cooling systems.

Figure 3 shows a 3D view of the cavity and a vector map of the magnetic field in the rectangular structure with four electrode pairs calculated by the code of CST MicroWave Studio (MWS). The distance between the centers of the neighboring pairs is about 10 cm and corresponds to a proton beam energy of ~25 MeV. It can be seen that the magnetic field encloses the electrodes and induces the

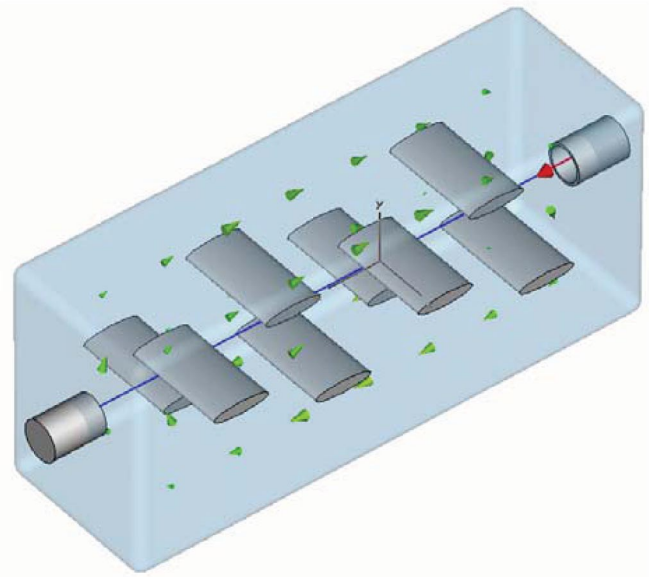

FIG. 3. (Color) 3D view of the rf deflector.

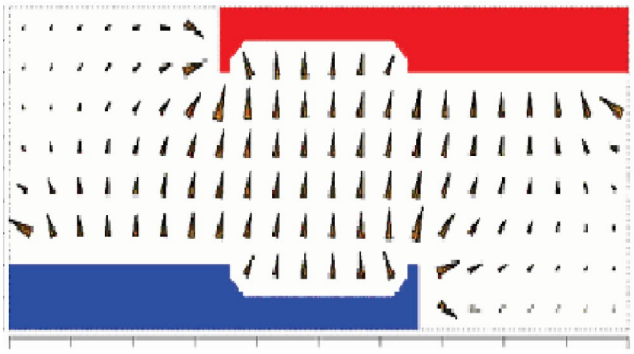

FIG. 4. (Color) Electrode shimming.

displacement current, which creates the induced electric field between the plates. Since the maximum field is usually in the middle of the capacitors, the ratio between the peak surface field and the maximum transverse component is in the range of $1 < E_{\mathrm{peak}}/E_{\perp}^{\mathrm{max}} < 2$. At the same time, it is desirable to have the homogeneous electric field distribution in the horizontal direction. For this purpose, we use the one-dimensional shimming (see Fig. 4). After correction, the field in the beam region has an irregularity $\pm 0.05\%$, which is quite satisfactory from the beam dynamics point of view.

Part of the magnetic flux penetrates the slots between the neighboring pairs. Therefore the electric field between the extreme plates is lower than in the center. Figures 5 and 6 show the electric and magnetic fields, respectively. Taking into account the harmonic time dependence, all these components, except the vertical component of the electric field, which is fundamental for the rf deflector, give a total effective kick close to zero. To additionally damp the vertical component of the magnetic field H_y an even number of electrode pairs should be chosen.

The nearest nonoperating mode is the TE102 mode with two variations along the cavity length. It has a frequency of

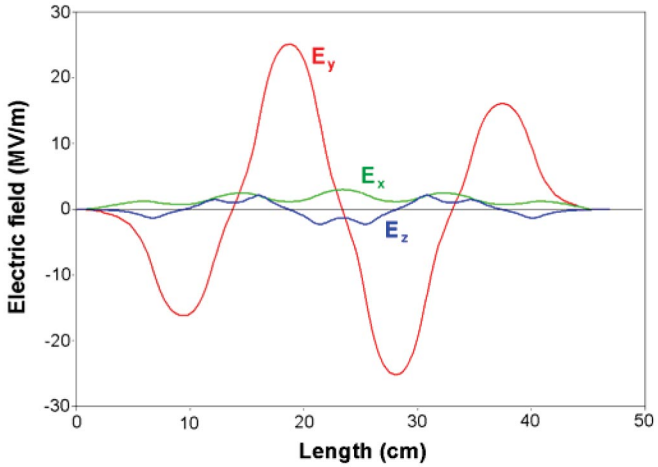

FIG. 5. (Color) Electric field.

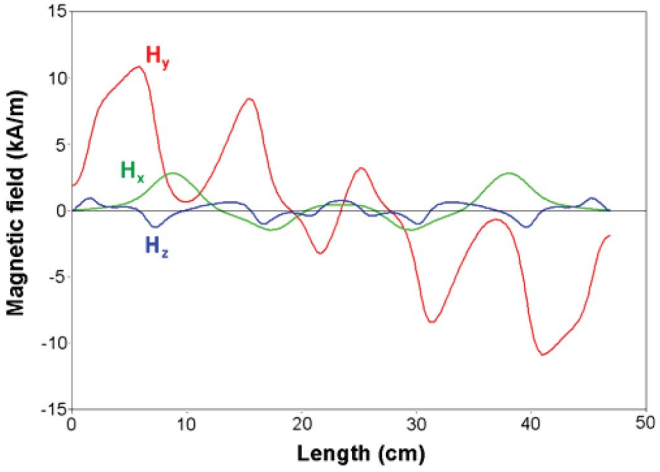

FIG. 6. (Color) Magnetic field.

~440 MHz, and it is far enough from the fundamental mode with a frequency of 352.2 MHz.

Three factors having an influence on rf deflector design are the deflection angle, the electrical maximum field, and the maximum rf power absorbed by the cooling system. The multielectrode device has a big advantage over the one-electrode device, since the deflection angle is proportional to the length of the device (number of electrode pairs), and we can obtain the necessary deflection angle by an appropriate choice of length. To characterize the specific power $P_{\rm rf}/L_{\rm def}$ required deflecting the beam by an angle α in the rf deflector with a length of $L_{\rm def}$ we introduce the efficiency $\text{eff} = \frac{\alpha^2 L_{\rm def}}{P_{\rm rf}}$ measured in the dimension of degree$^2 \cdot$ m/MW. Figure 7 shows the efficiency of the rf deflector versus the gap number for two frequencies 352.2 and 176.1 MHz at an energy of 25 MeV.

A significant gain of the 6–8 gaps (3–4 gaps for 176.1 MHz) over the one-gap device can be seen. But then the efficiency is almost constant, since with the deflection angle the space deviation grows with length as well, and the gaps have to be more and more open.

Figure 8 shows the transverse shunt impedance $R_{sh} = \frac{\bar{E}_{y,1}^2 L_{\rm def}}{P_{\rm rf}}$ versus the number of electrode pairs for the different structures, where $\bar{E}_{y,1}$ is the average first harmonic amplitude of the vertical field over the rf deflector length. First of all, we would like to note that our structure has more than one order higher shunt impedance. Second, in the case of the increasing aperture (low energy) the six-pairs option seems the most effective, and for the constant aperture (high energy) the shunt impedance remains almost constant. From these data it is easy to estimate the power generator required. For instance, for a deflection of 1° by the rf deflector with 6 electrode pairs and a length of ~70 cm, a power of ~8.0 kW is needed in the CW regime, which can be provided even by the solid-state generator.

IV. BEAM DYNAMICS

Let us assume the distribution of the electric field in the gap is described by $E_{x,y,z} = E_{x,y,z}(x, y, z)\cos[\omega t(z) + \varphi]$, where z is the longitudinal direction of the beam, y is the plane where we deflect the beam, x is the perpendicular direction, and φ is the rf phase. In our proposed rf-deflecting system we use the resonant structure, where the group velocity and Poynting's vector have to be equal to zero. Therefore the magnetic field has to be shifted to the quarter of wave in time and $H_{x,y,z} = H_{x,y,z}(x, y, z) \times \sin[\omega t(z) + \varphi]$. Then from the motion equation the angle and the coordinate of particles are changed as

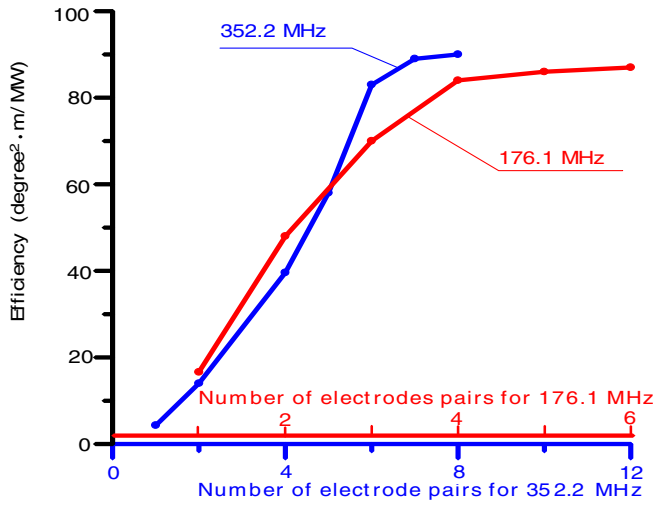

FIG. 7. (Color) Efficiency versus number of electrode pairs.

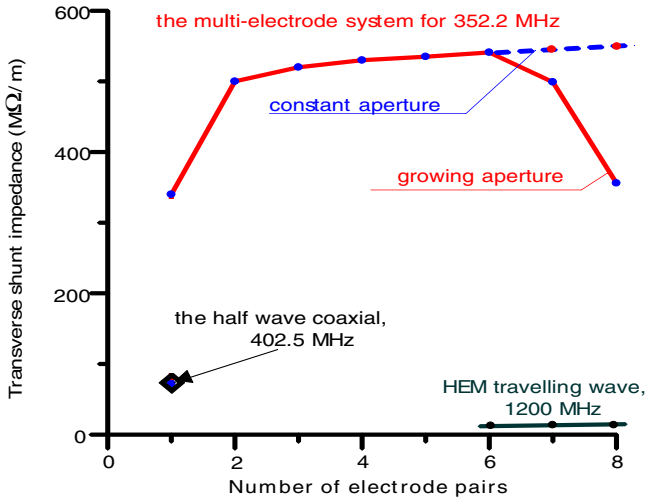

FIG. 8. (Color) Transverse shunt impedance for different structures.

$$\Delta\begin{pmatrix}\frac{dy}{dz}\\ \frac{dx}{dz}\end{pmatrix} = \frac{e}{m_0\gamma c^2\beta^2}\int_{-L_{\mathrm{def}}/2}^{L_{\mathrm{def}}/2} E_{y,x}(x,y,z)\cos[\omega t(z)+\varphi]dz + \frac{e}{m_0\gamma c\beta}\int_{-L_{\mathrm{def}}/2}^{L_{\mathrm{def}}/2}\mu_0 H_{x,y}(x,y,z) \times \sin[\omega t(z)+\varphi]dz, \Delta\begin{pmatrix}y\\ x\end{pmatrix} = \int_{-L_{\mathrm{def}}/2}^{L_{\mathrm{def}}/2}\Delta\begin{pmatrix}\frac{dy}{dz}\\ \frac{dx}{dz}\end{pmatrix}dz, \quad (1)$$

where λ is the wavelength, $c\beta$ is the velocity of the particles in the z direction, m and γ are the mass and the Lorenz factor, respectively. From Figs. 5 and 6, it can be seen that all components, except for E_y, make a negligible contribution to the final displacement of the beam from the axis. To minimize the harmful effect of H_y, which is estimated to be around a few percent of the E_y, the number of electrode pairs has to be even. Using the field Fourier series presentation, we can obtain $\Delta(\frac{dy}{dz}) = \frac{eE_{y,1}}{2m_0\gamma c^2\beta^2}\cdot \cos\varphi \cdot L_{\mathrm{def}}$. The y-deflection angle is therefore proportional to the first Fourier harmonic $E_{y,1}$ and to the deflector length. For the rectangular distribution of the function $E_y(x, y, z)$ versus z the angle has a maximum at $L_{\mathrm{def}} = \beta\lambda/2$, therefore this length is used in the half-wave coaxial deflector. In the common case, this is not correct since the distribution $E(x, y, z)$ is determined by the electrode geometry, which is optimized to achieve a maximum ratio between the first harmonic and the maximum surface field $E_{y,1}/E_{\mathrm{pick}}$.

In the periodical rf deflector the vertical field is changed as $E_y(x, y, z) = E_{y,1}(x, y)\cdot\cos kz$. If the space periodicity coincides with the rf period $kz = \omega t$, and the rf deflector has the length integer to the half-period $L = n\frac{\beta\lambda}{2}$, the deflection angle and space deviation are

$$\Delta\left(\frac{dy}{dz}\right) = \frac{eE_1\lambda\cdot n}{4m_0\gamma c^2\beta}\cdot\cos\varphi, \qquad \Delta(y) = \frac{eE_1\lambda^2\cdot n^2}{8m_0\gamma c^2}\cdot\cos\varphi. \quad (2)$$

Thus, the higher frequency factor can be quite easily compensated by increasing n.

Now let us discuss the emittance growth effect in the rf deflector. It can be seen from (2) that particle deflection depends on the rf phase φ. This is the most important factor causing emittance growth. If the required deflection angle of bunch is α, the rms transverse shift is $\langle\delta\mathrm{x}\rangle = \alpha\cdot L_{\mathrm{def}}\cdot\frac{1}{4}\langle\Phi^2_{\mathrm{bunch}}\rangle$, and the rms transverse kick is $\langle\delta\dot{\mathrm{x}}\rangle = \alpha\cdot\frac{1}{4}\times\langle\Phi^2_{\mathrm{bunch}}\rangle$, where $\langle\Phi^2_{\mathrm{bunch}}\rangle$ is the rms bunch phase length. Obviously, the particles are grouped around "0" and π phases, and the emittance growth is proportional to the average value of deviation from these phases:

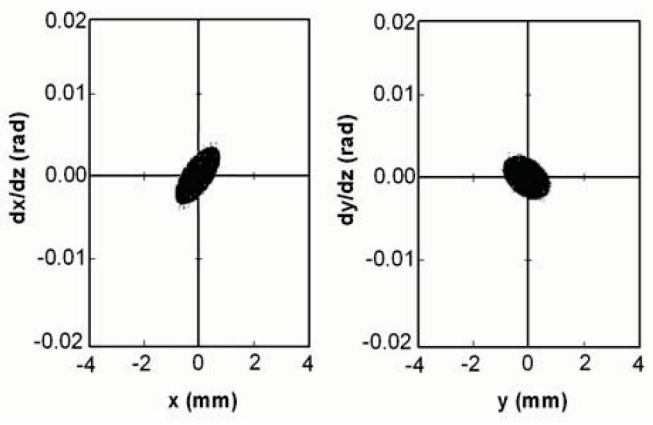

FIG. 9. Phase portrait in front of deflector.

$$\varepsilon_{\mathrm{eff}_{\mathrm{rms}}} = \varepsilon_{0\mathrm{rms}}\cdot\sqrt{1+\frac{\langle\delta\mathrm{x}\rangle^2}{\langle\mathrm{x}_{\mathrm{beam}}\rangle^2}+\frac{\langle\delta\dot{\mathrm{x}}\rangle^2}{\langle\dot{\mathrm{x}}_{\mathrm{beam}}\rangle^2}}, \quad (3)$$

where $\langle\mathrm{x}_{\mathrm{beam}}\rangle^2$, $\langle\dot{\mathrm{x}}_{\mathrm{beam}}\rangle^2$ are the rms beam sizes in the bunch center. Integrating the motion equation in the real 3D field calculated by MWS, we investigated this effect numerically. As an example, Figs. 9 and 10 show the phase portrait in front and behind the rf deflector with four electrode pairs at a beam energy of 25 MeV, bunch phase length $\Phi_{\mathrm{bunch}} = \pm 10^0$, and energy spread $\Delta W/W = \pm 0.1$. The emittance increases by $\approx 10\%$.

To reduce emittance growth, an rf deflector with inversion has been suggested [3]. Figure 11 illustrates this idea schematically. The rf deflector consists of two parts with mirror symmetry relative to the center. In the first part, the bunch is deflected in the required direction, and in the second part, due to the changed polarity of the electrodes, the bunch is slowed down to the initial transverse velocity $\frac{dy}{dz}|_{z=L_{\mathrm{def}}} = \frac{dy}{dz}|_{z=0}$.

Thus, the particles coming into the rf deflector leave it with the same divergence and with nonzero space deviation. The first aspect leads to emittance conservation, and the second is the required function of the rf deflector.

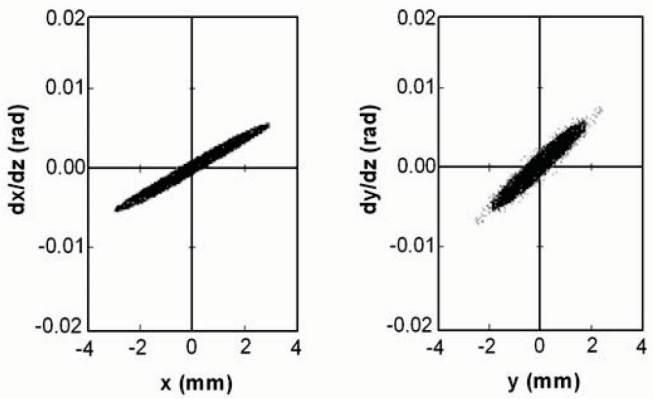

FIG. 10. Phase portrait behind deflector.

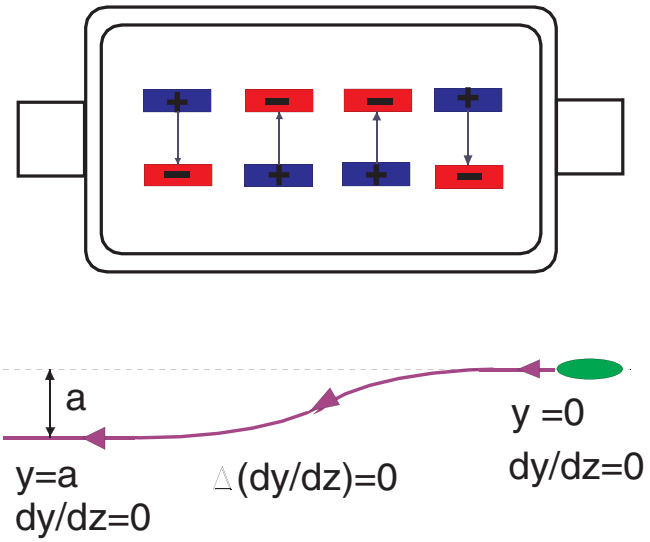

FIG. 11. (Color) The rf deflector with inversion.

We simulated this rf deflector numerically in order to confirm this positive feature. Figure 12 shows the phase portrait behind the rf deflector with the inverted second part. We can see that the emittance hardly increases at all.

V. FEATURES OF HIGH-FREQUENCY RF DEFLECTOR

We already mentioned above that our rf deflector can be used in an electron accelerator with the higher rf frequency of ~1000–1500 MHz. In principle, the period of such a deflector remains almost the same due to the higher relative velocity $\beta \approx 1.0$ and the shorter wavelength. However, for the higher energy $m_0c^2\gamma \approx 20$–30 GeV and the relatively low separation angle of ~1 mrad, the required rf deflector length has to be longer by factor ~3. Actually, the wavelength of the operating modes TE10p in the empty rectangular cavity with the height h is determined as $\lambda = 1/\sqrt{1/\lambda_{\text{cutoff}}^2 + (p/4l^2)2}$, where $\lambda_{\text{cutoff}} = 2h$ is the wavelength of the cutoff mode, $l = p\frac{\Lambda}{2}$ is the length of the resonator, and p is the variation number of the field along the resonator. Since the length of the resonator has to be an integer $m\frac{\beta\lambda}{2}$, then $\lambda/\lambda_{\text{cutoff}} = \sqrt{1-(p/m\beta)^2}$. Since the TE100 mode does not exist and the lowest index is $p = 1$, we can conclude that in the empty cavity the condition $1 \le p \le m$ must be fulfilled. Hence, the number of the electrode pairs determines the number of possible excited modes.

The nearest mode to the TE101 is the TE102 mode with a double variation of the field along the resonator [see Figs. 13(a) and 13(b)].

In the longer cavity, the probability of exciting the higher nonoperating mode is greater, and the mode spectrum is denser. With respect to the stability criteria, the frequency separation of two neighboring modes is the most important factor, and in our case at $f = 1200$ MHz it can easily be more than 5%. Analyzing all of these conditions, we suggest using TE101 as the operating mode in the H resonator sectioned into four pairs. The resonator consists of n sections fed separately by the generator. Each section includes four pairs of plates. The rf phase between the neighboring sections is 2π, which provides the resonant deflection of the beam. The length of one section is 50 cm with the period between the neighboring electrodes pairs being 12.5 cm. The width of the cavity is 3 cm and the height 6 cm. As an example, in order to deflect the electron beam with an energy of 20 GeV four half-meter sections

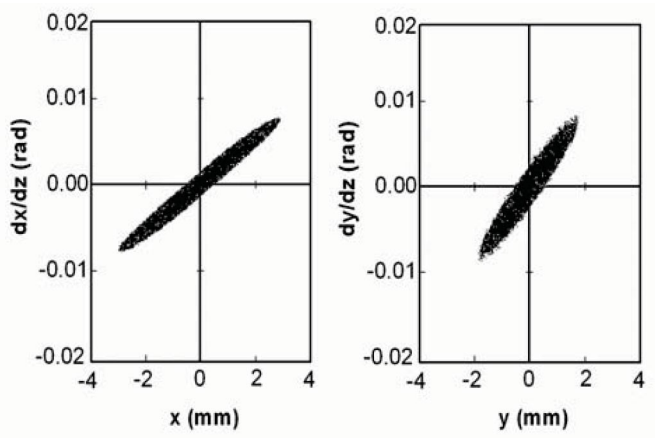

FIG. 12. Phase portrait behind deflector with inverted second part.

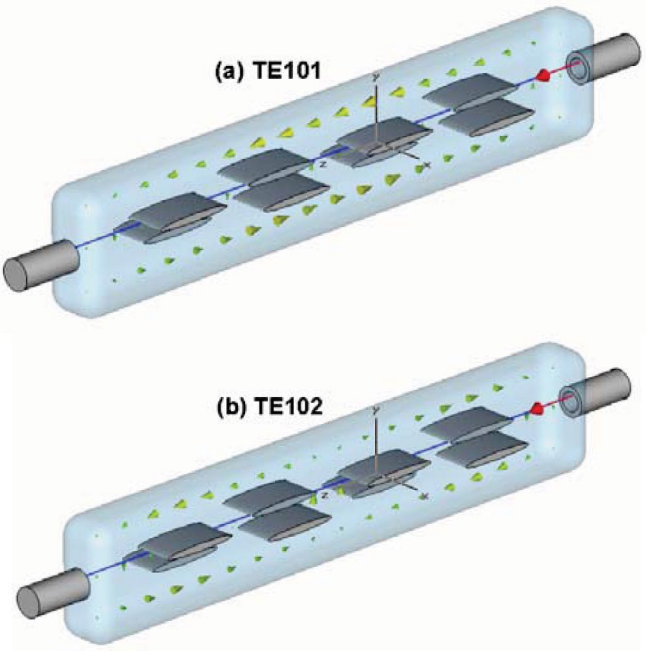

FIG. 13. (Color) TE101 (a) and TE102 (b) modes in the rf deflector for $f = 1200$ MHz.

with four electrode pairs and four 40 kW generators in the 10% duty cycle are needed for an angle of 1 mrad.

VI. EXPERIMENTAL PROTOTYPE OF RF DEFLECTOR

The results of the cavity prototype fabrication and experimental investigation are presented here. First of all, we determined the cavity sizes to obtain the required resonant frequency. In addition, we need to choose a deflecting plate material, which must operate without breakdown under an electric field strength of 30–35 MV/m with small surface resistance to ensure a high quality factor and with the vacuum equipment providing the operating pressure $5 \cdot 10^{-8}$ Torr. Experience with the design of the URAL-30M based on the H structure has shown that aluminum, aluminum alloys, and oxygen-free copper have a similar breakdown limit. At $E = 35$ MV/m the breakdown frequency does not exceed 0.02% [12]. Since the aluminum alloy electrode can be more easily manufactured, we used the aluminum alloy. To provide the operation pressure of $5 \cdot 10^{-8}$ Torr more easily within the rf deflector cavity a cylindrical shape was chosen for the test facility. The rate of outgassing for this vessel is $2 \cdot 10^{-10}$ L $\cdot$ Torr/s $\cdot$ cm^2. The vacuum seals and the rf contacts are made from indium. In testing, the vacuum pump provides a limit pressure of 10^{-10} Torr. The whole test facility is shown in Fig. 14. The ceramic BeO cap is used as the window to introduce the rf power and separate the air from the vacuum.

The feeder is terminated by the loop, and is placed in the cap. Such a unit was developed at the Institute of High Energy Physics (IHEP, Protvino), and is used in the RFQ accelerator. The indicator loop unit is similar to the previous one, but the size is smaller by a factor of 10. The unit for frequency tuning is described briefly in [12]. It has operated in the IHEP RFQ accelerator for a considerable time. The measured values of the relative electric field between the four pairs of deflecting plates are in the ratio of 0.8:1.0:1.0:0.8, which is in accordance with the MWS calculation.

During work with the experimental prototype the slice technology has been developed for the real rf deflector. Figure 15 shows the slices of the cavity with different shapes. They will be assembled in the cavity alternating the plate direction and inserting plateless slices.

VII. CONCLUSION

We developed the H-type rf deflector based on a new principle: the position of the deflecting electrodes is alternatively changed along the cavity and they produce the p-mode standing wave for the beam. The deflecting electrodes have the shape of the capacitor with the maximum electric field in the middle. Therefore the ratio between the peak surface field and the maximum transverse component is close to unity. Because of all these features our deflector has a transverse shunt impedance of 500–600 MΩ/m, which is more than one order higher in comparison with its analogues. The latter allows a lower power generator ~10 kW to be used instead of the MW-klystron system.

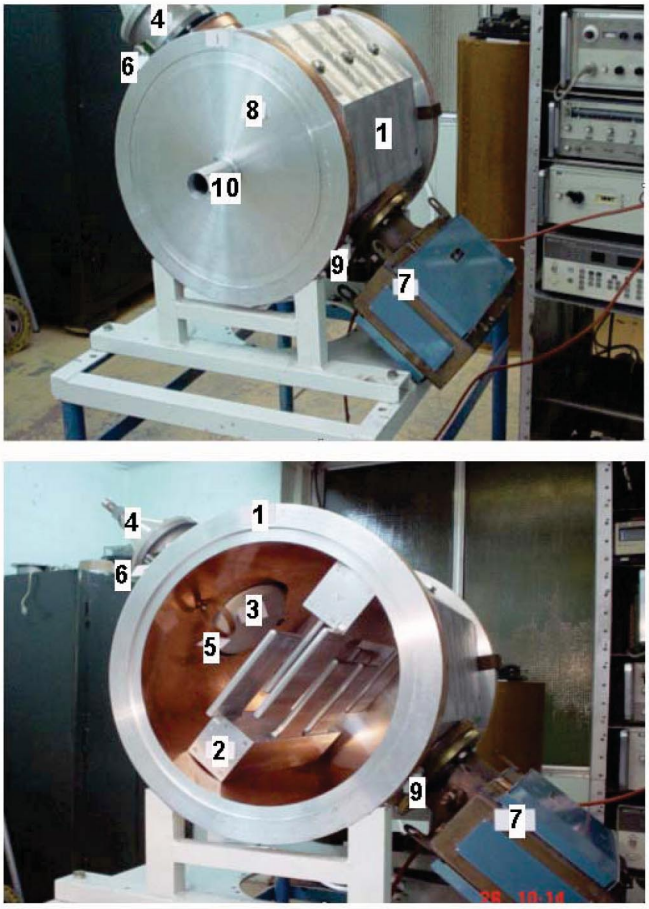

FIG. 14. (Color) The rf deflector test facility: 1—deflector container, 2—plate system, 3—ceramic window, 4—rf power unit, 5—copper ring, 6—unit of frequency tuning, 7—vacuum pump, 8—circular flange, 9—indicator loop, 10—beam pipe.

FIG. 15. (Color) Slices of the cylindrical and rectangular rf deflectors.

Thus, the H-type rf deflector meets all the requirements of the high duty cycle accelerator facility.

To minimize emittance growth an rf deflector with an inverted second part was developed, which can be regarded as the parallel beam shifter.

The simplicity of design and the high shunt impedance in a wide frequency range allow the device to be used in the proton (150–700 MHz) and electron machines (1000–1500 MHz).

We produced and tested the experimental prototype on the low rf power level. Using the prototype, we worked through the frequency tuning procedure. The proposed structure has a simple cooling system. In addition, the rf power input, the trimming unit, the indicator gauge, and the vacuum pump may be easily accommodated in the facility.

Altogether, this leads us to expect that the new device can be used for multipurpose applications.

[1] Yu. Senichev, Report No. ESS 103-00-A, 2000; in *Proceedings of 18th International Conference on High Energy Accelerators, HEACC'2001, Tsukuba, 2001*, http://conference.kek.jp/heacc2001/pdf/p2new06.pdf

[2] Yu. Senichev, Report No. ESS 110-01-A, 2001.

[3] Yu. Budanov *et al.*, ESS Report No. ESS 01-119-L, 2001; in *Proceedings of the European Particle Accelerator Conference, Paris, 2002* (EPS-IGA and CERN, Geneva, 2002), pp. 2196–2198, http://accelconf.web.cern.ch/AccelConf/e02/PAPERS/TUPLE091.pdf

[4] N. Pichoff, D. Uriot, W. Braeutigam, and Yu. Senichev, in *Proceedings of the Particle Accelerator Conference, Chicago, IL, 2001* (IEEE, Piscataway, NJ, 2001), pp. 3906–3908, http://accelconf.web.cern.ch/accelconf/p01/papers/FPAH098.pdf

[5] K. Bongardt and D. Sanitz, Primary Report Kernforschungszentrum Karlsruhe, No. 11 04 02P14C, 1982.

[6] L. S. Walling *et al.*, Report No. LA-CP-90.

[7] J. F. Stovall, F. W. Guy, R. H. Stokes, and T. P. Wangler, Nucl. Instrum. Methods Phys. Res., Sect. A **278**, 143 (1989).

[8] F. L. Kravczyk and S. Kurennoy, in *Proceedings of the 1999 Particle Accelerator Conference, New York, 1999* (IEEE, Piscataway, NJ, 1999), pp. 3588–3590, http://accelconf.web.cern.ch/AccelConf/p99/PAPERS/FRA84.PDF

[9] A. Schempp *et al.*, in *Proceedings of the Linac 1996 Conference, Geneva, 1996* (CERN, Geneva, Switzerland, 1996), pp. 47–49, http://linac96.web.cern.ch/Linac96/Proceedings/Monday/MOP01/Paper.html

[10] H. Zimmermann, A. Bechtold, A. Schempp, and J. Thibus, in *Proceedings of the Particle Accelerator Conference, Chicago, 2001* (Ref. [4]), pp. 3918–3920, http://accelconf.web.cern.ch/AccelConf/p01/PAPERS/FPAH103.PDF

[11] H. Hahn and H. J. Halama, Rev. Sci. Instrum. **36**, 1788 (1965).

[12] O. Belyaev *et al.*, in *Proceedings of the XX International Linac Conference, Monterey, 2000* (SLAC, Stanford, 2000), pp. 259–261, http://www.slac.stanford.edu/econf/C000821/MOD21.pdf